Molecular dynamics study of hydrogen isotopes at the Be/BeO interface

Etienne A Hodille, Jesper Byggmästar, Yves Ferro, Kai Nordlund

Postprint accepted for publication in Journal of Physics: Condensed Matter:
https://doi.org/10.1088/1361-648X/ac8328

Molecular dynamics study of hydrogen isotopes at the Be/BeO interface

E A Hodille[1], J Byggmästar[2], Y Ferro[3], K Nordlund[2]

[1] CEA, IRFM, F13108 Saint Paul Lez Durance, France
[2] Department of Physics, University of Helsinki, P. O. Box 43, FI-00014,Finland
[3] Aix Marseille Université-CNRS, PIIM UMR 73450, 13397 Marseille, France

E-mail: `etienne.hodille@cea.fr`

Abstract. Molecular dynamics simulations are used to investigate the behaviour of D atoms at two interfaces between Beryllium (Be) and Beryllium oxide (BeO). After relaxation of the simulation cell, there are (i) localised defects at the interface and (ii) a hexagonal misfit dislocation network creating a succession of compressed and expanded area from each side of the interface. The simulations between 750 K and 1500 K for tens to hundreds of nanoseconds show that both interfaces act as trapping sites for D atoms. The simulations also show that D atoms tend to migrate in the material where the hydrogen isotope solubility is the highest as predicted by thermodynamics. However, the simulations also shows that there are additional kinetic barriers (D trapping sites, D_2 formation/dissociation in BeO) that slow down the path to equilibrium. These additional kinetic barriers may influence the fuel retention and permeation in Be materials.

Keywords: Plasma-wall interactions, Molecular Dynamics, material interface, hydrogen

1. Introduction

The material chosen for the first wall of JET [1, 2] and ITER [3] tokamaks is Beryllium (Be). During the tokamak operation, Be materials may interact with the plasma mainly composed of deuterium (D) and tritium, two hydrogen isotopes (from hereon called HI). These interactions lead to the retention of HI in Be materials, either in the first wall or in codeposited layers which are the main media for fuel retention expected in ITER [4, 5]. This HI inventory is detrimental for the tokamak operation for control and safety reason. Indeed, in ITER, there is an operation limit for the total in-vessel inventory of 700 g. In addition, the retention and uncontrolled release of the fuel trapped in the materials can have problematic effects on the core plasma control especially during long pulse operations [6]. Thus, the knowledge of retention properties of hydrogen isotopes in Be materials are of prime importance to quantify the impact of plasma-wall interactions on plasma operations.

Modelling can be used at different scales to predict and anticipate how HI reacts with Be and BeO materials. At atomistic scale, the fundamental interactions of HI with Be materials are obtained with density functional theory (DFT) [7, 8, 9, 10, 11, 12, 13] or molecular dynamics (MD) [14, 15, 16, 17, 18]. The outputs of these atomistic simulations can then be used in higher scale methods such as reaction diffusion model [19] or Kinetic Monte Carlo [16] that can be used to simulate migration and trapping of fuel in Be at experimental length and time scales.

Investigations led so far on the Be-O-H system either focus on Be only [7, 8, 9, 10, 14, 15, 16] or BeO [11, 12, 17, 18]. However, Raman spectroscopy of JET plasma facing materials [20, 21] shown inclusion of BeO in Be in codeposited layers. Thus, it is important to understand how HI behaves at the interface between Be and BeO.

Regarding the interaction of HI at other material/material interfaces, early experimental investigations in steels suggest that HI can be trapped at TiC particles/Fe interface [22, 23]. The suggested mechanism is trapping at misfit disclocation networks at the interface between both materials [23] which is also the case for trapping of HI at NbC particles in steel [24]. DFT calculations also suggest that HI can be trapped by various interfaces such as Fe/cementite [25], W/WC [26], Fe/W [27], Ta/Li [28] or bcc Fe/Y_2O_3 [29] due to a reduction of the solution energy near the interface.

The purpose of this paper is to investigate the possible trapping of HI at the Be/BeO interface with the MD method. Both materials have lattices with hexagonal symmetry (hcp for Be and wurtzite for BeO). The experimental study of the growth of BeO on top of Be(0 0 0 1) with electron diffraction and electron microscopy suggests that the first stage of BeO growth is in the $\langle 0\,0\,0\,1\rangle$ direction with $\langle 1\,0\,0\,0\rangle$ of Be and BeO being parallel [30]. Thus, in our study we will first build interfaces between Be(0 0 0 1) and BeO(0 0 0 1) that satisfy these conditions. Then, HI will be randomly inserted in either Be or BeO materials and simulations between 10 and 100 ns will be run with MD to investigate the evolution of the system at temperatures between 750 K and 1500 K.

2. Method

Experiments of BeO growth on Be suggest that at the Be(0 0 0 1)/BeO(0 0 0 1) interface, $\langle 1\,0\,0\,0\rangle$ directions of Be and BeO are parallel [30]. However, there is a mismatch between both lattice constants in this direction: $a_{\mathrm{Be}} = 2.25 - 2.32$ Å [31] and $a_{\mathrm{BeO}} = 2.698 - 2.766$ Å [32]. Thus, having an interface satisfying the symmetry of both lattices implies creating a big enough supercell. To do that, we are using classical molecular dynamics and the code PARCAS [33]. The OVITO software [34] is used for the visualisation of the positions of the atoms and the plots are done with matplotlib [35].

2.1. Interatomic potentials

The simulation cells contain three species: Be, oxygen (O) and deuterium (D). We use deuterium as it is the main plasma particle used in current tokamaks. To describe the interactions between atoms, Tersoff-like potential [36, 37] are used. For these interactions, D atoms are considered as H atoms with a mass of 2.014 atomic mass units. Thus, a kinetic process such as diffusion characterized by a rate k will be affected through $\frac{k_{\mathrm{D}}}{k_{\mathrm{H}}} = \sqrt{\frac{m_{\mathrm{H}}}{m_{\mathrm{D}}}}$, with m_X the mass of the hydrogen isotope X. The Be-O-H ternary potential we previously established is given in [17] and combines Be-Be and Be-H potential from [31] (version II), the H-H potential from [38], the O-O potential from [39],

the Be-O potential from [32] and the O-H potential from [17].

2.2. Simulation set-up

2.2.1. Geometry of the interface To simulate the interface between Be(0 0 0 1) and BeO(0 0 0 1), a BeO wurztite sub-supercell with a thickness $z_{\mathrm{BeO}} = 45$ Å is inserted in the center of a Be hcp sub-supercell of thickness $z_{\mathrm{Be}} = 112$ Å. A similar method is used in [40] to simulate the Fe/FeO interface. The thickness of the BeO layer is much smaller than the Be one in order to simulate the realistic case where a thin layer of BeO grows on top of bulk Be.

For both cells, $\langle 0\,0\,0\,1\rangle$ are parallel to the **z** direction. Thus, the system is Be/BeO/Be with two Be/BeO interfaces which allows to apply periodic boundary conditions in the **z** direction. Such boundary conditions prevent the escape of added D atoms by any open surfaces as periodic boundary conditions are also applied in **x** and **y** directions.

As there is no plane of symmetry perpendicular to $\langle 0\,0\,0\,1\rangle$ for the BeO wurtzite structure, both interfaces are not equivalent: for the BeO(0 0 0 1) surface, Be terminates the surface while it is O for the BeO$(0\,0\,0\,\bar{1})$ surface. For sake of clarity, in the following, only the indices of the BeO planes are given: the studied interfaces are the Be/BeO$(0\,0\,0\,\bar{1})$ interface and the Be/BeO(0 0 0 1) interface.

The simulation cells used in this study have a rectangular cross section of 72×76 Å^2 in the $(\mathbf{x}, \mathbf{y})$ plane, with **x** being aligned in the $\langle 1\,0\,0\,0\rangle$ direction of both Be and BeO lattices. In principle, this is not the smallest box size which would guarantee a match between the Be and BeO cells in **x** and **y** direction. However, when looking at the simulation cell from the top (figure 1), one can see a pattern with almost hexagonal symmetry appearing due to the lattice mismatch. This pattern is higlighted by the red hexagons in figure 1 which show places where the Be lattice is almost perfectly aligned with the BeO lattice. The chosen dimensions of the cells in the $(\mathbf{x}, \mathbf{y})$ plane are the smallest dimensions that guarantee the hexagonal symmetry of this pattern beyond the border of the cell as periodic boundary conditions are applied in **x** and **y** directions. With these dimensions, the match is not perfect between the Be hcp sub-supercell and the BeO wurtzite sub-supercell: the Be sub-supercell is 0.3 % bigger than the BeO one in the **x** direction and the BeO sub-supercell is 0.1 % bigger than the Be one in the **y** direction.

2.2.2. Relaxing the interface Before adding any D atoms in the system, we have to ensure that the interfaces are in a low energy configuration that would represent a realistic system. First, the simulation cell is annealed during 1 ns with the temperature in the system maintained at 1500 K using a Berendsen thermostat [41] on all atoms. During this step, a pressure control is applied to the system (at 0 Pa). After this initial step, the system evolves for another 1 ns but with no temperature and no pressure control. Finally, the system is quenched to 0 K in 10 ns using temperature and pressure control. During these three steps, the time step for integration is 0.3 fs.

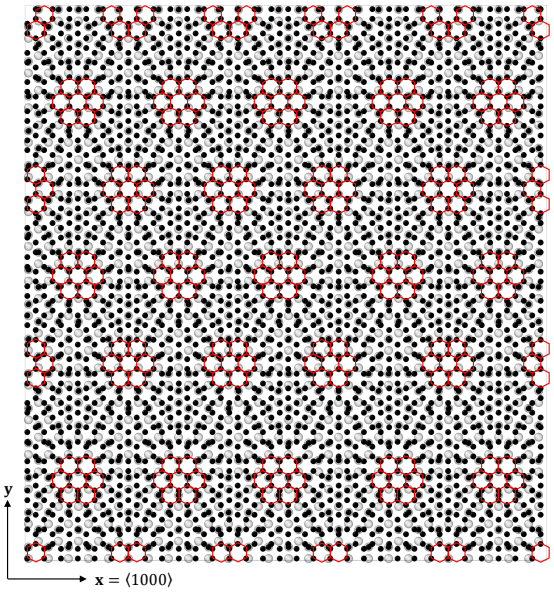

Figure 1: Top view of the 72×76 Å^2 simulation cell (prior to relaxation) in the $(\mathbf{x}, \mathbf{y})$ plane. Gray spheres represent the positions of the O atoms while black spheres represent the positions of Be atoms. **x** is parallel to $\langle 1\,0\,0\,0\rangle$ of both the Be and BeO lattices. The red hexagons show places where the Be lattice is almost perfectly aligned with the BeO lattice.

2.2.3. Adding D to the material After the relaxation, the behaviour of D atoms at the Be/BeO interface is investigated. At a given temperature T, the relaxed simulation cell is first annealed for 10 ps at the temperature T using the temperature control on all atoms as well as a pressure control (at 0 Pa). Then D atoms are inserted either in the Be or BeO part of the simulation cell with a desired initial concentration c_{D}^0 which is chosen to be around 0.5×10^{28} Dm^{-3} (≈0.05 atomic fraction). This high concentration is used to have a significant amount of D added to the simulation cells which improves the likelyhood of events. The studied temperatures ranges between 750 K and 1500 K in order to speed up the kinetics of the involved processes.

The most stable position of hydrogen isotopes in Be is the basal tetrahedral site (BT) [7, 8, 10]. Thus, to insert D in Be, we randomly select a Be atom in the Be part, calculate the coordinates of one of the BT neighbouring sites and put a D atom at these coordinates. In BeO, there are multiple stable configurations involving single HI or HI_2 molecules [12] with HI_2 being the most stable. However, it requires the bonding of two HI for HI_2 to be formed in BeO, which may be limited by the HI diffusion if HI is initially inserted in the atomic form. Thus, in the BeO part, D atoms are inserted at random positions with a constraint on the initial minimum D-D distance ($\geq$ 0.7 Å) and D-O/Be distance ($\geq$ 1.15 Å). These constraints prevent artificial recoil energy deposition due to the short range repulsion when starting the MD simulation. These constraints also allow the formation of all the possible configurations of D in BeO, including D_2 in the initial cell. However, with the chosen concentration, the quantity of D_2 stays low in this initial cell and mostly atomic D is inserted in BeO.

After D atoms are inserted either in Be or in BeO, the simulation cell is again relaxed for another 10 ps at the desired temperature with a pressure control. Then, the system is simulated for several nanoseconds to study the diffusion and segregation of HI at the interface. For the simulations of D initially in Be, the simulations last 20 ns which is enough to observe a significant evolution of the system thanks to the fast diffusion of D in Be. The temperature control is applied to a 12 Å-thick slab in the centre of the simulation cell in order to be far enough from any D atoms so their velocity are not re-scaled by the thermostat. For the simulations of D initially in the BeO, the simulations last 120-130 ns because the diffusion of D in BeO is much slower. The temperature control is applied to 10 Å-thick slab in the bottom of the slab which is far enough from the zone of interest so no velocity of atoms near the interface is re-scaled by the thermostat. For all these simulations, the time step for integration is 0.1 fs.

2.2.4. Physical quantities To assess the quality of the interface as well as the evolution of the amount of D in the materials, we look at the profiles, in the $\mathbf{z}$ direction, of the average concentration of the species $X \in \{\text{Be, O, D}\}$ and of the average potential energy per atom (in eV/atom). To do that, we consider a slice of thickness Δz centred at the coordinate z. In that slice, the concentration of the specie X (m^{-3}) is:

$$c_X = \frac{N_X}{S\Delta z} \tag{1}$$

where N_X is the amount of atoms X in the slice and $S = 72 \times 76$ Å^2 is the cross section in the $(\mathbf{x}, \mathbf{y})$ plane. The concentration can also be defined in atomic fraction (at.fr.) as:

$$c_X = \frac{N_X}{\Sigma_I N_I} \tag{2}$$

where $\Sigma_I N_I$ is the total amount of atoms in the slice. Similarly, the average potential energy per atom is:

$$E_{\text{pot}} = \frac{\Sigma_i E_{\text{pot},i}}{\Sigma_I N_I} \tag{3}$$

where $E_{\text{pot},i}$ (eV) is the potential energy of the atom i with i iterating over all atoms in the slice.

Several stable configurations exist for D in BeO [11, 12] with the molecular configuration being the most stable [12] which depends on their environment (O, Be or D). To distinguish between these configurations and also to distinguish if a D atoms is in Be or BeO, the element of the nearest neighbours (O, Be or D) is detected. This allows to calculate the number of D close to O ($N_{\text{O-D}}$), to Be ($N_{\text{Be-D}}$) or bound to another D (N_{D_2}). To correctly detect the D_2 molecules (which should give an even number of D atoms) a D_2 is detected as soon as the D-D distance is below 1.1 Å. Thus, we are taking into account the possible vibrating molecules for which the D atoms are closer to the Be/O lattice atoms. More details about the method to accurately detect D_2 molecules is given in appendix A.

3. Results

3.1. Analysis of the interface

3.1.1. Compressed/expanded material The simulation cell (without D) obtained at the end of the relaxation procedure is shown in different planes in figure 2. For the view in the $(\mathbf{x}, \mathbf{z})$ and $(\mathbf{y}, \mathbf{z})$ planes, what is shown in figure 2 is a 5 Å-thick slice in the perpendicular direction positioned at the centre of the simulation cell. In these two views, if the distance between 2 Be atoms is below 2.25 Å, a bond is created by OVITO.

In a pure relaxed Be, with the used interatomic potential, the Be-Be distance is 2.33 Å (in the hexagonal basal plane) and 2.26 Å (out of the hexagonal plane). Having Be-Be distances lower than 2.25 Å means the Be is compressed in this area. After relaxation, these compressed areas exhibit periodicity (figure 2(b) and (c)) with the same hexagonal symmetry as the pattern shown in figure 1: they are caused by the misalignment between the Be and BeO lattice at the interface. Between the compressed area, close to the interfaces, the material is expanded compared to perfect Be. These expanded area are where the Be and BeO lattice are almost aligned (see the red hexagons in figure 1).

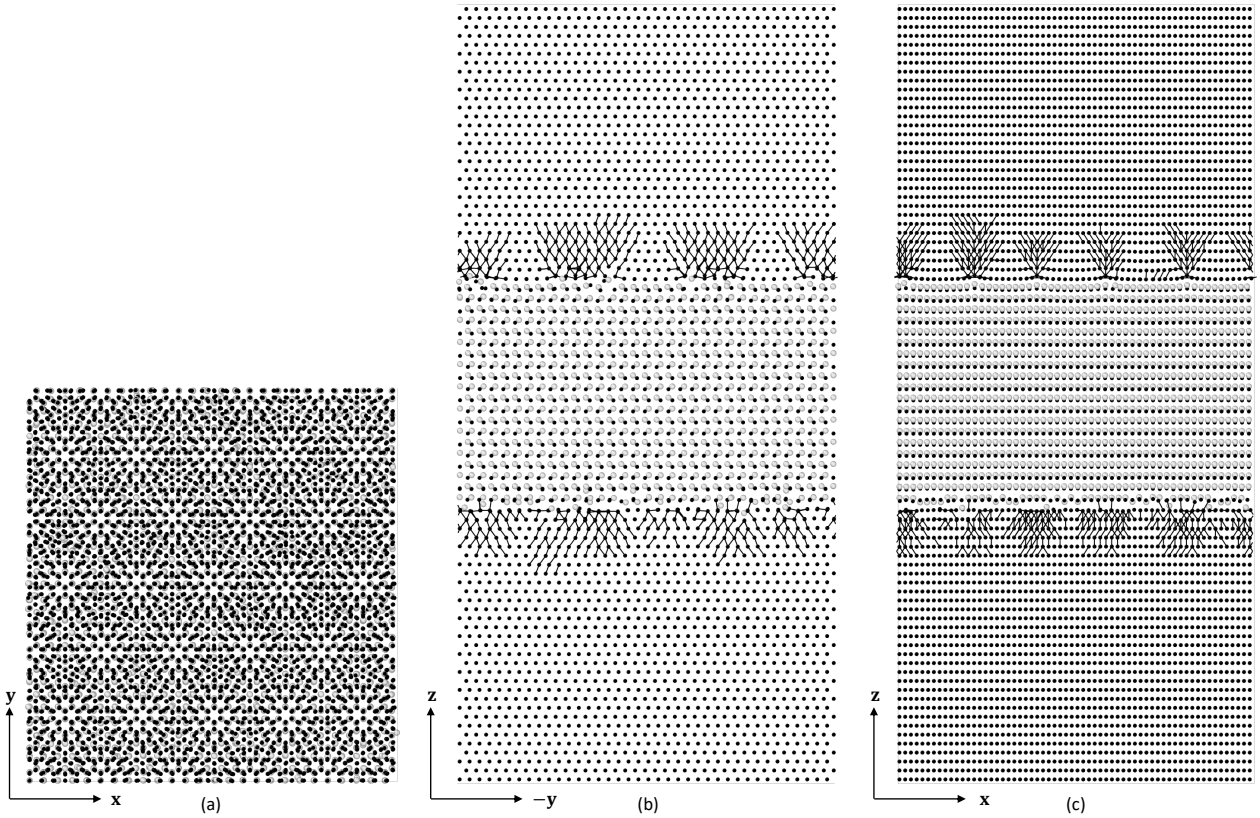

Figure 2: The simulation cell after the relaxation procedure, viewed from the top in the $(\mathbf{x}, \mathbf{y})$ plane (a), from the side in the $(\mathbf{y}, \mathbf{z})$ plane (b) and from the side in the $(\mathbf{x}, \mathbf{z})$ plane (c). For the side views (b) and (c), only a slice of 5 Å thick in the perpendicular direction is shown, positioned at the center of the simulation cell. In these slices, the bonds represent the places where the Be-Be distance is below 2.25 Å. Gray spheres represent the positions of the O atoms and black spheres give the positions of Be atoms.

3.1.2. Misfit dislocation network To further analyse the compressed/expanded area we used the dislocation analysis tool of OVITO [42] on the last frame of the relaxation procedure. The analysis is done only on the Be atoms considering the hcp structure as input crystal (Be atoms in wurtzite also have symmetry of the hcp structure). It reveals two different networks of misfit edge dislocations in the interface planes. Both networks are shown in figure 3 for the Be/BeO$(0\,0\,0\,\bar{1})$ interface (a) and for the Be/BeO$(0\,0\,0\,1)$ interface (b).

At the Be/BeO$(0\,0\,0\,\bar{1})$ interface, the Burgers vector of the dislocations is $\frac{1}{3}\langle 1\,\bar{2}\,1\,0\rangle$. The dislocation lines form hexagons centred on the place where Be and BeO lattices match. In figure 2 (c), the first plane of Be atoms in contact with BeO$(0\,0\,0\,\bar{1})$ (top interface) has a periodic bump indicating the position of the edge dislocation. A similar hexagonal pattern of misfit dislocation with the same Burgers vector was observed at the Ti$(0\,0\,0\,1)$/TiN$(1\,1\,1)$ interface studied with MD [43, 44].

At the Be/BeO$(0\,0\,0\,1)$ interface, the Burgers vectors of the dislocations are mostly $\frac{1}{3}\langle 1\,\bar{1}\,0\,0\rangle$ forming rough equilateral triangles which, once assembled, form hexagons. However, for this interface, the network is much more chaotic which is accompanied by many point defects at the interface as one can see in figure 2(b) and (c) (bottom interface).

The difference between the networks comes from the specie terminating BeO$(0\,0\,0\,\bar{1})$ or BeO$(0\,0\,0\,1)$. BeO$(0\,0\,0\,\bar{1})$ is terminated by O atoms which ensure a strong adhesion to the Be atoms of the metallic layer. It is worth noting that the above mentioned Ti/TiN interface observed the same hexagonal misfit dislocation network for N terminated layers in contact with Ti [44]. On the other hand, BeO$(0\,0\,0\,1)$ is terminated by Be atoms. Thus, the O atoms below them tends to be attracted by the metallic Be creating defects in addition to the misfit dislocations, as observed at the bottom interface in figure 2 (b) and (c). The nature of these defects can be described as

O vacancies in the top most layer at the BeO(0 0 0 1) surface and O interstial atoms at the Be/BeO(0 0 0 1) interface. To show further the difference between the interfaces, one can define the thickness of the interface as the distance between the plan of Be atoms that terminate the pure Be and the plane of atoms that terminates the BeO part (either Be or O atoms for BeO(0 0 0 1) and BeO(0 0 0 $\bar{1}$) respectively). This thickness of the Be/BeO(0 0 0 $\bar{1}$) interface is about 1.6 Å and the thickness of the Be/BeO(0 0 0 1) interface is about 2.3 Å.

3.1.3. Atomic concentrations and potential energy Figure 4 (a) shows the evolution of the concentration of Be and O in the simulation cell along the z coordinate. As expected, $c_{\mathrm{Be}} = 1$ in metallic Be and $c_{\mathrm{Be}} = c_{\mathrm{O}} = 0.5$ in the oxide layer. Also, the c_{Be} decrease is thicker at the Be/BeO(0 0 0 1) interface than at the Be/BeO(0 0 0 $\bar{1}$) interface due to the difference in element terminating the BeO planes, as previously discussed.

Figure 4 (b) reports the evolution of the potential energy per atom along the z coordinate. Far away from the interface, E_{pot} matches well the potential energy of the perfect hcp or wurtzite structures (horizontal dashed lines): the simulation cell is big enough to represent a realistic configuration of a thin BeO layer connected to Be bulk. At both interfaces, the potential energy is climbing up from E_{pot} (-5.559 eV/atom) in perfect BeO to E_{pot} in perfect Be (-3.62 eV/atom). These intermediates layers are where the concentration of Be and O are not equal and where there are interface defects. Then, in the Be part, right next to the interfaces, there are small bumps of E_{pot} related to the compression/expansion of the Be lattice shown in figure 2 (b) and (c). Since the potential energy per atom is averaged on all atoms of one slice, the amplitude of the bump is only ≈ 0.03 eV. However, some individual atoms have potential energy of about -2.90 eV at the Be/BeO(0 0 0 $\bar{1}$) interface and -3.20 eV at the Be/BeO(0 0 0 1) interface, compared to -3.63 eV in perfect Be.

3.2. D inserted in metallic Be

3.2.1. Local evolution of the D concentration First, D is inserted in the metallic Be parts with a concentration of 0.05 at.fr. which represents an addition of 3475 D atoms. figure 5 shows the simulation cell at the beginning (a) and after 10 ns at 1000 K (b). Initially, the D is uniformly distributed in the Be material and after 10 ns, a clear agglomeration of D is observed at the interfaces and no D has crossed the interfaces to reach BeO. At the Be/BeO(0 0 0 $\bar{1}$) interface, the D seems to be agglomerated following a regular pattern along the interface. This pattern is

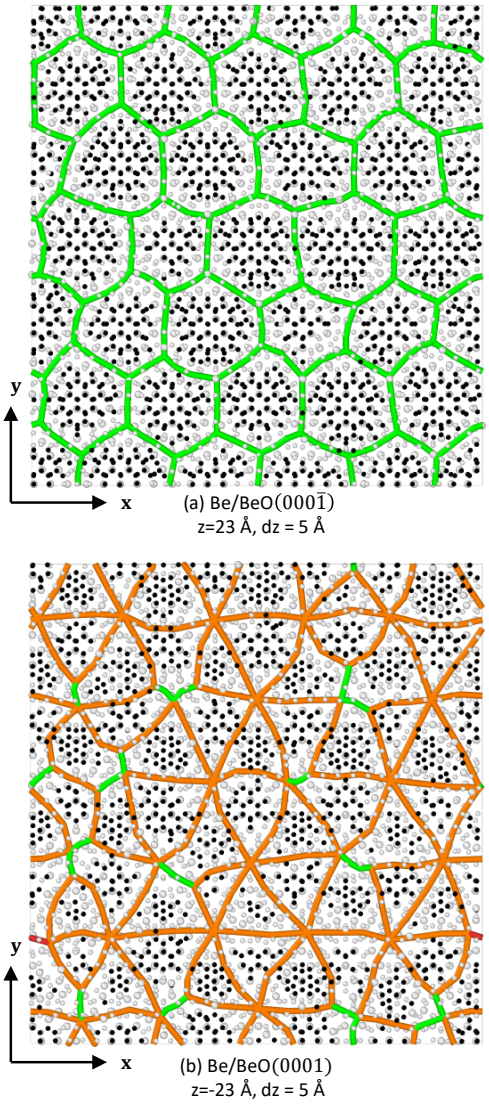

Figure 3: Misfit dislocation network at the Be/BeO(0 0 0 $\bar{1}$) interface (a) and at the Be/BeO(0 0 0 1) interface (b). To see the dislocation networks at the interfaces, only slices of $\Delta z = 5$ Å at $z = 23$ Å and at $z = -23$ Å are shown. The green lines are edge dislocations with $\frac{1}{3}\langle 1\,\bar{2}\,1\,0\rangle$ Burgers vector and the orange ones are edge dislocations with $\frac{1}{3}\langle 1\,\bar{1}\,0\,0\rangle$ Burgers vector. The black atoms represents the atoms that considered to be part of a hcp lattice by OVITO and the grey atoms are the non-hcp atoms used when OVITO finds the dislocation lines.

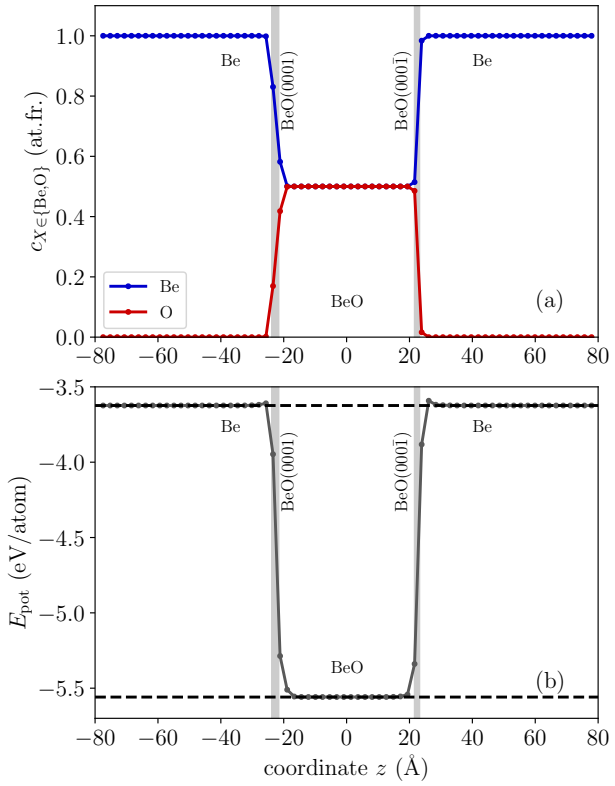

Figure 4: (a) average concentration c_X (at.fr.) of the specie $X \in \{\mathrm{Be}, \mathrm{O}\}$ at the coordinate z. (b) average potential energy per atom at the coordinate z. The vertical grey areas show where the interfaces are: their thicknesses represent the thicknesses of the interfaces as defined in section 3.1.1. The horizontal dashed lines at -5.559 eV/atom and -3.62 eV/atom in (b) show the 0 K potential energies of the perfect BeO or Be structures respectively. 0 eV potential energy represents an atom which is not bound to any other atoms (in the cutoff range of the interatomic potentials). The profiles are obtained with a slice thickness $\Delta z = 2.25$ Å.

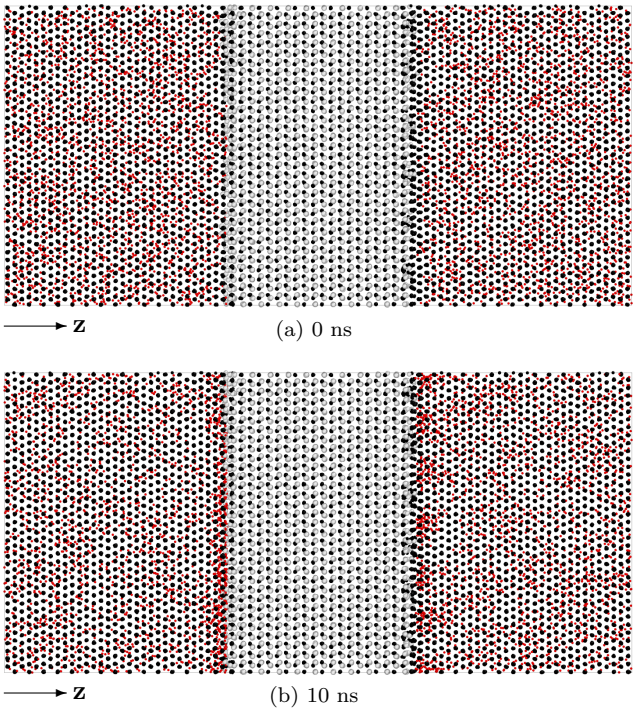

Figure 5: Simulation cells a $t = 0$ ns (a) and $t = 10$ ns (b) after the insertion of a concentration of 0.05 at.fr. ($\approx 5 \times 10^{27}$ D/m^3) in the metallic Be at 1000 K. The positions of Be, O and D are given by the black, grey and red spheres respectively. The **z** direction is also represented in order to identify the Be/BeO(0 0 0 1) interface (left) and the Be/BeO(0 0 0 $\bar{1}$) interface (right).

due to the misfit dislocation network highlighted earlier in section 3.1. The misfit dislocations create expanded and compressed area in Be and D atoms sits preferably in the expanded part while they tend to stay away from the compressed one.

In order to quantify the evolution of the D trapped at the interface, the concentration of D, c_{D}, is calculated with equation 1 and $\Delta z = 2$ Å. Figure 6 shows the D profile at the beginning and at the end of the 20 ns MD simulations at 750 K (a), 1000 K (b) and 1250 K (c). At the beginning of the simulations, the concentration of D varies slightly around 0.5×10^{28} Dm^{-3}. After 20 ns of simulations, the agglomeration of D can be observed right next to the interfaces without any D crossing the interface toward the BeO part. This agglomeration spans over two to three slices of 2 Å. For the Be/BeO(0 0 0 1) interface, the D is trapped at the interface thanks to the defects created there. For the Be/BeO(0 0 0 $\bar{1}$) interface, the D is trapped on a broader range and one slice away from the interface: the D atoms sit in the expanded Be area near the interface.

The agglomeration of D at the interface is accompanied by a small decrease of the D bulk concentration (far away from the interface). At 1000 K and 1250 K (figure 6((b)-(c)), the bulk concentration remains uniform in the material thanks to the fast diffusion of D in Be at these temperatures. Conversely, at 750 K (figure 6(a)), the bulk concentration is not uniform and the depletion is pronounced next to where D atoms are trapped. It creates a gradient of D concentration which should eventually be removed thanks to diffusion from bulk. However, this diffusion is not fast enough at 750 K to be triggered efficiently on the time and length scale of the simulation.

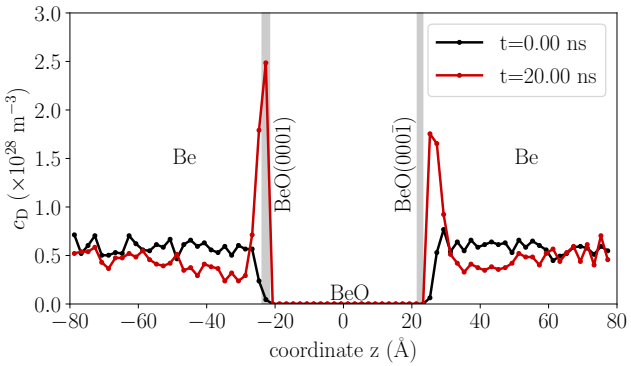

(a) 750 K

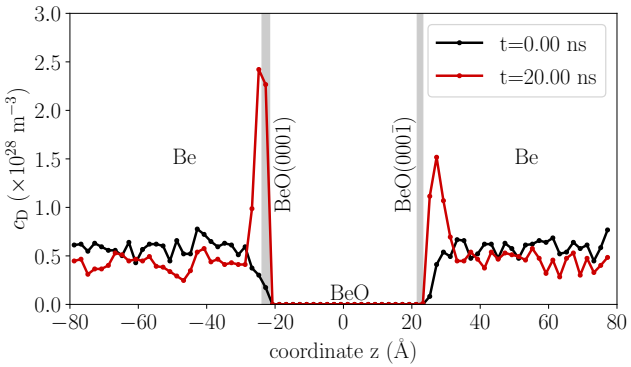

(b) 1000 K

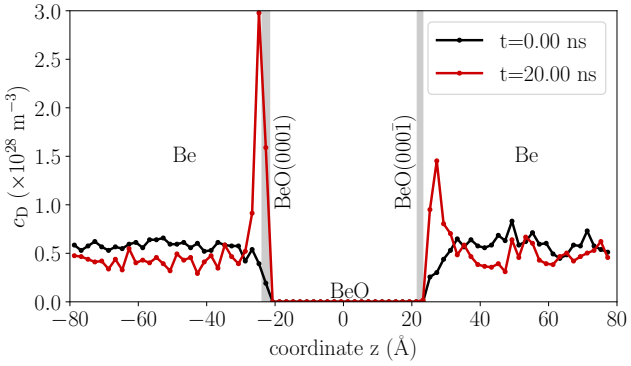

(c) 1250 K

Figure 6: Profiles of the concentration of deuterium c_D at 0 and 20 ns along the **z** direction for the MD simulations at 750 K (a), 1000 K (b) and 1250 K (c). c_D is calculated using equation 1 with $\Delta z = 2$ Å. The horizontal gray lines represent the positions of both interfaces.

3.2.2. Kinetics of D trapping at the interfaces To investigate the kinetics of the D trapping at the interface, the amount of D atoms trapped at the interface, $N_{\text{D trapped}}$, is defined as the amount of D in the three slices with the highest concentrations right next to the interfaces. The evolution of this quantity with time is reported in figure 7 at the Be/BeO(0 0 0 1) interface (a) and at the Be/BeO(0 0 0 $\bar{1}$) interface for the simulation at 750 K, 1000 K and 1250 K.

For both interfaces and temperatures, $N_{\text{D trapped}}$ increases with time and tends to saturate after a few ns of simulation. This is typically the results of a balance between trapping and detrapping which depends on the local concentration of interstitial particles, the content of free trapping sites and the temperature. In particular,the kinetics is faster at higher temperature: the saturation is not reached at 750 K but it is at 1250 K. In addition, the total quantity of trapped D seems lower at higher temperature, at least for the agglomeration of D at the Be/BeO(0 0 0 $\bar{1}$). Both observation indicated the presence of a trapping process thermally activated.

At all temperatures, the amount of D trapped by the Be/BeO(0 0 0 1) interface is a bit higher than the amount of D retained near the Be/BeO(0 0 0 $\bar{1}$) which is also seen on the concentration profile (figure 6). At both temperatures, the interfaces retained about 300-600 D atoms and since the cross-section of the simulation cell is 72×76 Å^2, the retention at the interface represents 5-9×10^{18} D/m^2, i.e. about one monolayer, in a slice 6 Å thick.

3.3. D inserted in BeO

3.3.1. Local evolution of the D concentration D is now inserted in the BeO slab with a concentration of 0.05 at.fr. which represents an addition of 1642 atoms. Because D diffusion is slower in BeO than in Be, the simulations had to be pushed up to 120-130 ns and the temperature above 1250 K in order to be able to see significant evolutions of the system.

Figure 8 and figure 9 show the concentration of D at the beginning (a) and the end (b) of the simulations at 1500 K and 1250 K respectively. The average D concentration in the BeO part at the beginning and at the end of the simulations are also shown in black and grey dashed lines respectively. For both temperatures, most of the D are bound to an oxygen atoms at the beginning of the simulations, as it is the most stable configuration of dissolved atomic D in BeO with the used potential [17]. Some D_2 are also present in a much lower amount as well as very few Be-D.

At the end of the simulation at 1500 K, D have been transferred to the Be part thanks to the steep D gradient at the interface. Thus, the amount of Be-D rises but is only present in the Be part. And the

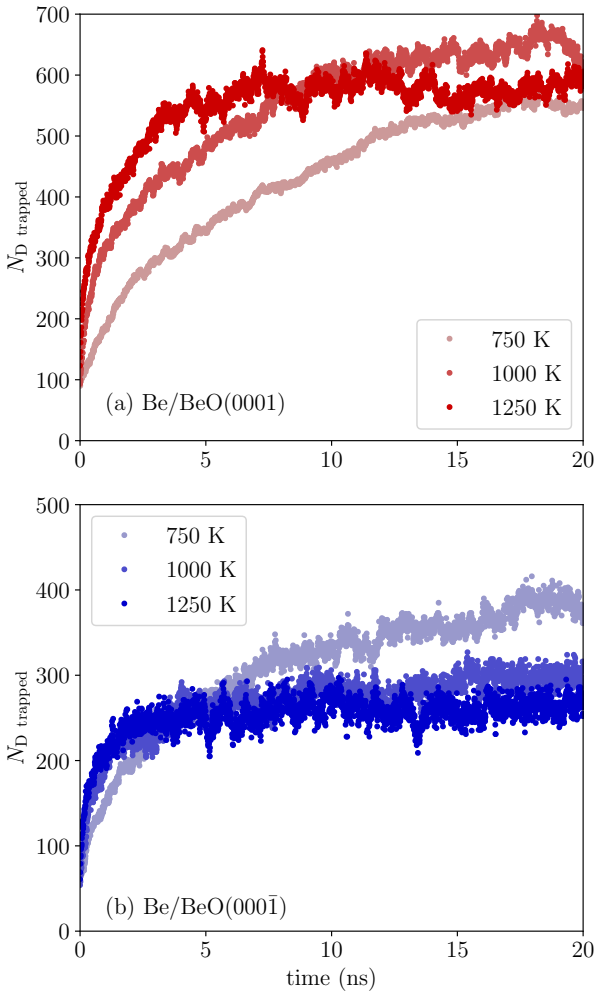

Figure 7: Amount of D trapped, $N_{\mathrm{D\ trapped}}$, at the Be/BeO(0 0 0 1) interface (a) and at the Be/BeO(0 0 0 $\bar{1}$) interface (b) during the MD simulation at 750 K, 1000 K and 1250 K. $N_{\mathrm{D\ trapped}}$ is the amount of D in the three slices (each with $\Delta z = 2$ Å) next to the interfaces.

concentration of Be-D is higher near the interfaces due to the trapping sites highlighted in section 3.2. In the BeO part, there is a conversion of O-D bond into D_2 molecules as D atoms diffuse close to each other. And this conversion seems more pronounced at the interfaces especially at the Be/BeO(0 0 0 1) (around -20 Å). This interface may acts as a trap for D_2, though it is not a bubble of gas as the D concentration remains low. In the simulation at 1250 K, similar behaviour can be observed but the temperature being lower, the kinetics of all the processes are much slower.

3.3.2. Kinetics of D transport across the interface
To investigate the kinetics of D transport across the

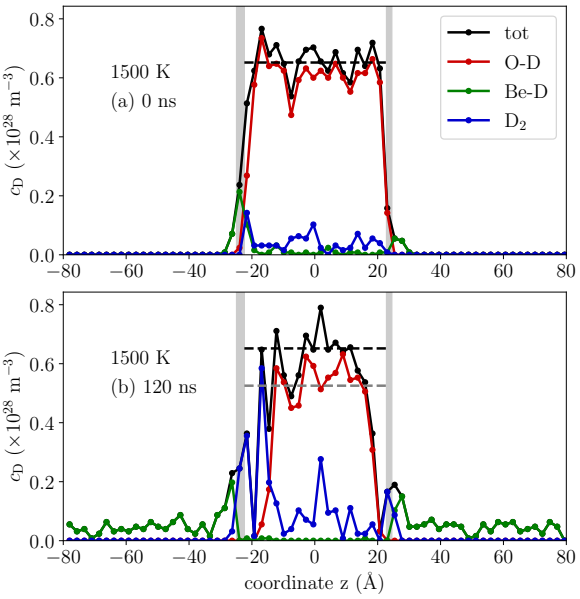

Figure 8: Deuterium concentration c_{D} along the **z** direction at 0 ns (a) and 120 ns (b) after the introduction of an initial concentration of D (0.05 at.fr.) in the BeO slab at 1500 K. The position of the interface and their thicknesses are represented by the grey vertical lines. The slice thickness to calculate the concentration is $\Delta z = 2.35$ Å. The black and grey vertical dashed lines show the averaged deuterium concentration in the BeO part at the beginning and end of the simulations respectively.

Be/BeO interface, we look at the evolution of the number of D in each binding configuration. Figure 10 shows the evolution of $N_{\mathrm{O-D}}$ (a), $N_{\mathrm{Be-D}}$ (b) and $N_{\mathrm{D_2}}$ (c) for both simulated temperatures.

The amount of $N_{\mathrm{O-D}}$ decreases with time while both $N_{\mathrm{D_2}}$ and $N_{\mathrm{Be-D}}$ increase. The growth of $N_{\mathrm{D_2}}$ shows that D atoms tend to bond to other D in BeO as soon as the migration of atomic D is triggered. This is thermally activated as one can see that the growth of $N_{\mathrm{D_2}}$ at 1250 K is much slower than at 1500 K. Looking at the depth profile (figure 8/ 9), this growth is largely enhanced by the presence of the interface, either by speeding up the D transport in this area and thus increasing the probability of meeting between two D or by the presence of traps.

The growth of $N_{\mathrm{Be-D}}$ and the decrease of $N_{\mathrm{O-D}}$ is an indication that D will tend to transport across the Be/BeO interface when initially positioned inside the BeO materials. One can also observed an apparent saturation of $N_{\mathrm{Be-D}}$ in the simulation at 1500 K which does not seem to happen for $N_{\mathrm{D_2}}$. At the early stage of the simulations, there are atomic D bound to O at the interfaces that can either recombine to form D_2 or

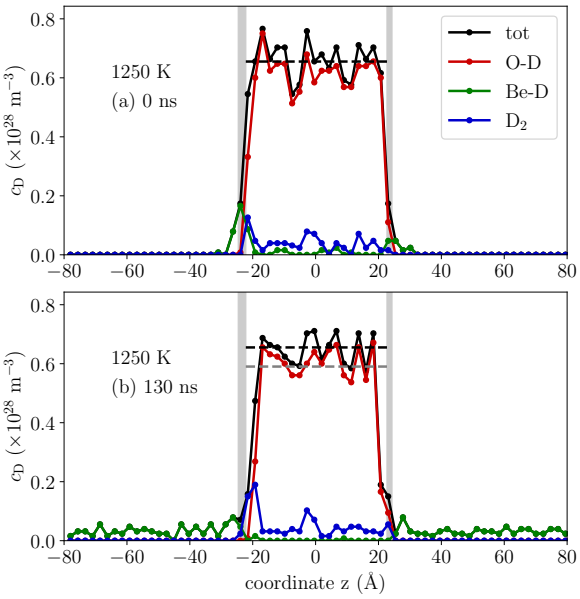

Figure 9: Deuterium concentration c_D along the **z** direction at 0 ns (a) and 130 ns (b) after the introduction of an initial concentration of D (0.05 at.fr.) in the BeO slab at 1250 K. The position of the interface and their thicknesses are represented by the grey vertical lines. The slice thickness to calculate the concentration is $\Delta z = 2.35$ Å. The black and grey vertical dashed lines show the averaged deuterium concentration in the BeO part at the beginning and end of the simulations respectively.

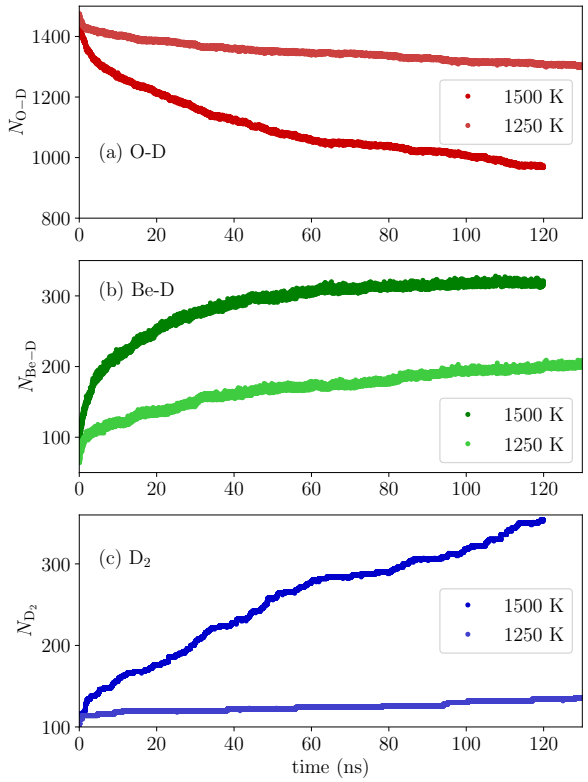

Figure 10: Total amount of D as O-D (a), Be-D (b) and D_2 (c) during the MD simulations at 1250 K and 1500 K.

cross the interfaces. Once all of these O-D near the interfaces are consumed, there are only D_2 near the interfaces (figure 8) (b). The fact that the growth of Be-D stops then is an indication that at the time scale of the simulation, D_2 do not dissociate at the interface which blocks the transfer of D from BeO to Be.

4. Discussion

4.1. Thermodynamic considerations

In macroscopic rate equation models of HI transport in plasma facing components with multi-materials, different models exists to tackle the transfer across the interface. For instance, one can use the continuity of the concentration of mobile (interstitial) HI or the continuity of the chemical potential [45, 46, 47, 48] at the interface. The latter model is based on Thermodynamics and is the most physical one. When the HI solubility in the materials from each side of the interface are different, it implies a discontinuity of the concentration of interstitial HI which can be modelled by the following Nernst distribution law:

$$\frac{c_1}{c_2} = \frac{S_1(T)}{S_2(T)} \tag{4}$$

with c_i the HI concentration in the material i (in m^{-3}) and $S_i(T)$ (m^{-3}Pa$^{-1/2}$) the temperature dependent HI solubility in the material i. Following this model, if the solubility of HI in material 1 is higher, the concentration of HI in this material tends to be higher than in material 2.

The solution energy of HI in Be in the BT site calculated by DFT is in the 1.40 eV - 1.67 eV range [7, 8, 9, 10] and is 1.35 eV within the interatomic potential used in this study [31]. The solution energy of HI in BeO calculated by DFT is 1.98 eV/H for neutral H_2, 3.31 eV for charged state at the pinning level and about 4.00 eV for neutral atomic H [12]. Within the interatomic potential used in this study, it is 1.69 eV/H for H_2 and higher than 2.04 eV for any configurations involving atomic H [17]. In all the cases, the solution energy of HI in Be is lower than the solution energy of HI in BeO. Thus, neglecting at the first order the entropic effect, one should expect a higher concentration of HI in Be than in BeO. The ratio

between both concentrations can be estimated with the solution energy as:

$$\frac{c_{\mathrm{H}}^{\mathrm{BeO}}}{c_{\mathrm{H}}^{\mathrm{Be}}} \approx \exp\left(-\frac{E_{\mathrm{H}}^{\mathrm{BeO}} - E_{\mathrm{H}}^{\mathrm{Be}}}{k_{\mathrm{B}}T}\right) \quad (5)$$

with $k_{\mathrm{B}} = 8.617\times10^{-5}$ eV/K, the Boltzmann constant, T the temperature and E_{H}^{i} the solution energy of HI in the material i (Be or BeO). Taking the values obtained for the interatomic potential, one should expect a ratio between 0.02 (H_2 in BeO/H in Be) and 0.0003 (H in BeO/H in Be) at 1000 K.

When 3475 D atoms are inserted in Be at 1000 K, one could expect about 66 D atoms in the BeO as D_2 molecules and no atomic D. In the MD simulations, none are observed in BeO which qualitatively agrees with the prediction. The small difference can be explained by the kinetics aspect: To appear as D_2, the D atoms have first to meet at the interface and bind there or cross the interface as atomic D (which is not probable according to equation 5) and bind inside BeO.

When 1642 D atoms are inserted in BeO at 1500 K, one could roughly expect about 100 D atoms as D_2 and 8 as atomic D at equilibrium. This is not what is observed because the system is kinetically limited by the slow diffusion [12, 49] of D in BeO (as atomic D or D_2) which is much slower than D diffusion in Be [10]. However, the trend agrees with the interface model of equation 5: the D atoms tend to cross the interface toward metallic Be. One should also mention that the formation of D_2 may block the transport of D from BeO to Be as soon as it becomes the main D configuration at the BeO side of the interface. Indeed, the D_2 would need to first dissociate before crossing the interface which adds another kinetic process.

To conclude on the interface model based on equation 4, it is a good approximation as soon as the kinetic exchanges between materials from each side of the interface are fast compared to the time constant of the other processes in the calculations (trapping, diffusion and permeation). At the time scale of these MD calculations, it seems the thermodynamic equilibrium is beyond reach even at temperature as high as 1500 K. In addition, in the particular case of the Be/BeO interfaces, the presence of D_2 may block the exchange at the interface by adding an additional kinetic barrier.

4.2. Trapping at the interface

4.2.1. Nature of the trapping sites In these MD simulations, especially when D is inserted in Be, agglomeration of D is observed at the interfaces. It is due either to the presence of defects at the interfaces or to the misfit between both materials leading to compressed and expanded area where D can be trapped.

In other materials, the presence of energy wells for HI (traps) at the interfaces such as Fe/cementite [25], Fe/Y_2O_3 [29] or W/Fe [27] have been calculated by DFT methods and our MD simulations show the same process occurring at the Be/BeO(0 0 0 1) interface. Another trapping process at the interface involves the misalignment of lattice materials from each side of the interface. Such misalignment creates a misfit dislocation network which creates compressed and expanded area especially visible in the Be part (figure 7(c)). The MD simulations show that D tends to agglomerate where the Be lattice is expanded and is absent where the Be is compressed. It results in an agglomeration of D near the Be/BeO(0 0 0 $\bar{1}$) interface. This trapping mechanism has also been described for HI at the W/WC interface [26] with DFT calculations and the trapping of HI at misfit dislocations is suggested to explain experimental results on HI trapping at carbide particles in steels [23, 24].

This trapping aspect is not taken into account in the current macroscopic models implementing equation 4. Indeed, this model assumes that the thermodynamic equilibrium is quickly reached which is a heavy assumption in presence of strong kinetic barriers such as traps at the interface. The presence of such trapping mechanisms is important to take into account for the estimation of HI inventory in multi-material components as our MD calculations show that the interface can retain about 10^{19} D/m^2 (which is equivalent to a monolayer of D adsorbed on a surface). It could also delay the permeation of HI across such components.

4.2.2. Rate equation modelling In the appendix of [47], a kinetic description of HI at the interface is proposed with trapping sites at the interface. From this kinetic description, a rate equation (RE) model is built. The steady-state of this RE model is compatible with equation 4 but it renders the transient increase of the concentration of HI at the interface. With this model, the concentration of HI at the interface increases and saturates with the same behaviour as the growth of $N_{\mathrm{D\ trapped}}$ in figure 7, when imposing a constant concentration in one side of the interface. This model is used to analyse further the MD simulations results when D is inserted in Be (section 3.2). The MD results when D is inserted in BeO are not analysed because the formation of D_2 is not taken into account in the RE model.

To analyse the results of the MD simulations presented in section 3.2, the RE model is simplified, based on the observations made in the MD simulation, assuming:

(i) no gradient of D: the diffusion is fast enough to

Table 1: Temperature dependent rate constants (s^{-1}) of the form $\nu_{x\to y}(T) = \nu_0 \exp\left(-\frac{E_{x\to y}}{k_B T}\right)$ for trapping and detrapping at the interface derived from the rate equation modelling (see the dashed line in figure 13).

	$\nu_{\mathrm{Be}\to\mathrm{i}}(T)$		$\nu_{\mathrm{i}\to\mathrm{Be}}(T)$	
	ν_0 (s^{-1})	$E_{\mathrm{Be}\to\mathrm{i}}$ (eV)	ν_0 (s^{-1})	$E_{\mathrm{i}\to\mathrm{Be}}$ (eV)
Be/BeO(0 0 0 1)	3.285×10^{10}	0.231	4.104×10^{9}	0.229
Be/BeO(0 0 0 $\bar{1}$)	3.217×10^{10}	0.229	1.877×10^{10}	0.292

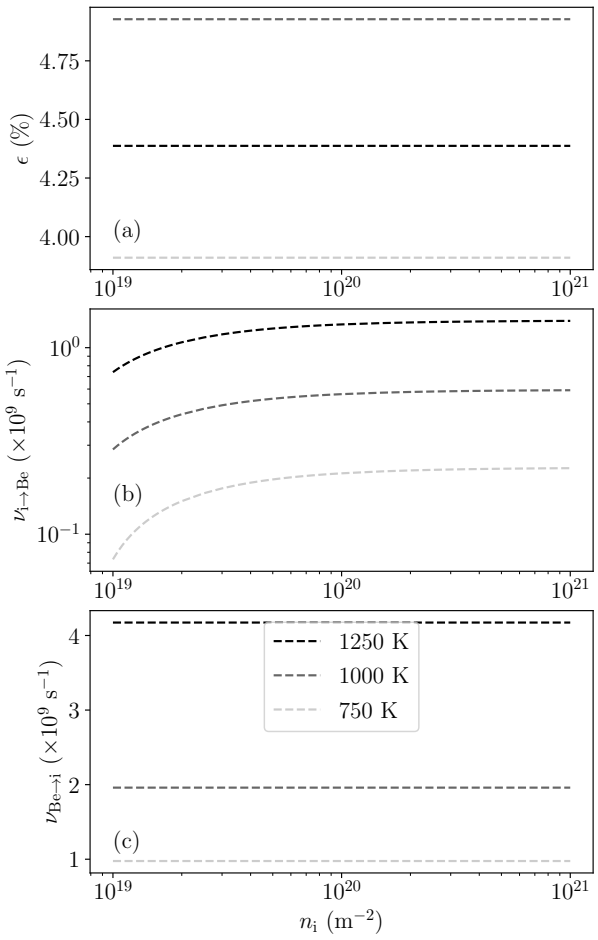

Figure 11: For the RE modelling of D trapping at the Be/BeO(0 0 0 $\bar{1}$) interface, evolution of the minimum error ϵ (in %) (a) and optimised reaction rates $\nu_{\mathrm{i}\to\mathrm{Be}}$ (b) and $\nu_{\mathrm{Be}\to\mathrm{i}}$ (c) for various values of n_{i} between 10^{19} m^{-2} and 10^{21} m^{-2}.

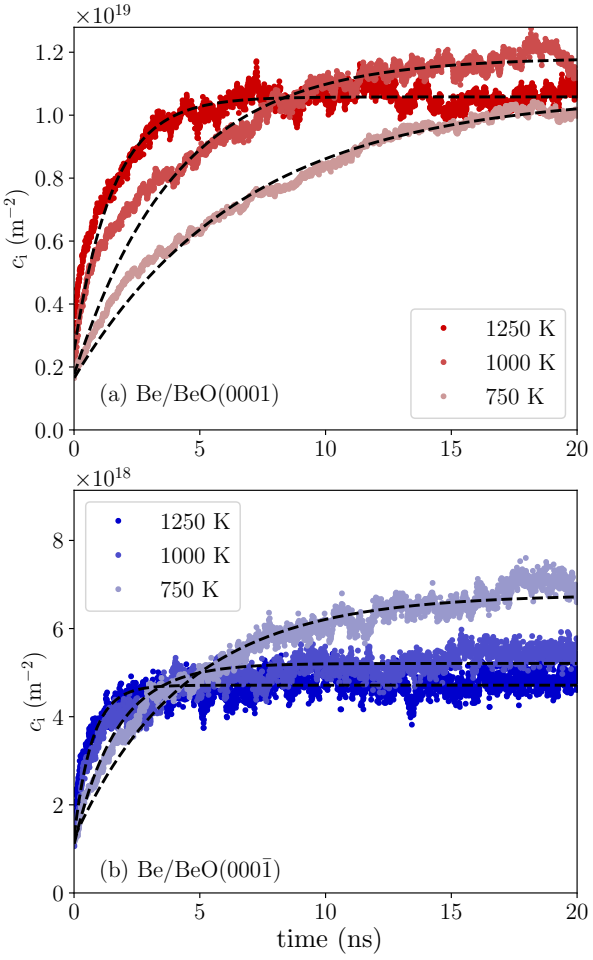

Figure 12: Evolution of the D concentration trapped at the interface c_{i} in the MD simulations (dots) and given by the rate equation model (black dashed line) with optimised parameters for the Be/BeO(0 0 0 1) (a) and Be/BeO(0 0 0 $\bar{1}$) (b) interfaces.

homogenise the D concentration in Be,

(ii) no D passing in the BeO as observed in the MD simulations,

(iii) the concentration of D in Be stays constant (figure 6): the reservoir of D in Be is high compared to the accumulation of D at the interface. This concentration stays equal to $c_{\mathrm{Be}} = 5 \times 10^{27}$ m^{-3}.

All these assumptions simplify the RE model to a single trapping/detrapping equation giving the evolution of the concentration of D at the interface c_{i} (m^{-2}):

$$\frac{dc_{\mathrm{i}}}{dt} = \nu_{\mathrm{Be}\to\mathrm{i}}(T)\,(1-\theta_{\mathrm{i}})\,\lambda_{\mathrm{Be}}c_{\mathrm{Be}} - \nu_{\mathrm{i}\to\mathrm{Be}}(T)c_{\mathrm{i}} \tag{6}$$

where $\lambda_{\mathrm{Be}} = 2 \times 1.577$ Å is the jumping distance between two interstitial sites in Be [10] (so $\lambda_{\mathrm{Be}}c_{\mathrm{Be}}$ is the areal density of interstitial D which interacts with the interface). The interface coverage is $\theta_{\mathrm{i}} = \frac{c_{\mathrm{i}}}{n_{\mathrm{i}}}$ (dimensionless between 0 and 1) with n_{i} (m^{-2}) the amount of trapping sites at the interface. The temperature dependent rate constants for trapping and detrapping from the interface are $\nu_{\mathrm{Be}\to\mathrm{i}}(T)$ and $\nu_{\mathrm{i}\to\mathrm{Be}}(T)$ (s^{-1}) respectively.

This ordinary differential equation can be solved analytically and the time evolution of c_{i} is:

$$c_{\mathrm{i}}(t) = c_{\mathrm{i}}^{\infty}\left[1 - \exp\left(-\frac{t - t_{\mathrm{delay}}}{\tau_{\mathrm{i}}}\right)\right] \tag{7}$$

with c_{i}^{∞} (m^{-2}) the steady-state concentration of D at the interface, τ_{i} (s) the characteristic time constant and t_{delay} (s) a time delay linked to the initial concentration of D at the interface as:

$$t_{\mathrm{delay}} = \tau_{\mathrm{i}} \ln\left(1 - \frac{c_{\mathrm{i}}(t=0)}{c_{\mathrm{i}}^{\infty}}\right). \tag{8}$$

Both c_{i}^{∞} and τ_{i} are expressed as a function of the trapping parameters at the interface:

$$c_{\mathrm{i}}^{\infty} = \frac{n_{\mathrm{i}}}{1 + \frac{\nu_{\mathrm{i}\to\mathrm{Be}}n_{\mathrm{i}}}{\nu_{\mathrm{Be}\to\mathrm{i}}\lambda_{\mathrm{Be}}c_{\mathrm{Be}}}} \tag{9}$$

$$\tau_{\mathrm{i}} = \frac{c_{\mathrm{i}}^{\infty}}{\nu_{\mathrm{Be}\to\mathrm{i}}\lambda_{\mathrm{Be}}c_{\mathrm{Be}}}. \tag{10}$$

To determine the temperature dependence of the reaction rates, the growth of c_{i} observed in the MD simulations is simulated with equation 7. For each temperature and interface, there are three free parameters: n_{i}, $\nu_{\mathrm{Be}\to\mathrm{i}}$ and $\nu_{\mathrm{i}\to\mathrm{Be}}$. For a set of these parameters, the quality of the RE model is quantified with the relative error $\epsilon = \frac{\int |c_{\mathrm{i}}^{\mathrm{MD}}(t) - c_{\mathrm{i}}^{\mathrm{RE}}(t)|dt}{\int c_{\mathrm{i}}^{\mathrm{MD}}dt}$. The free parameters, except for n_{i}, are determined using a similar parametric optimisation as in [50] based on the optimize.minimize function of the scipy package [51, 52].

Figure 11 shows the sensitivity of the minimised error (a) and optimised reaction rates (b-c) to the parameter n_{i} between 10^{19} m^{-2} and 10^{21} m^{-2} for the Be/BeO(0 0 0 $\bar{1}$) interface (the exact same behaviour happens for the Be/BeO(0 0 0 1) interface). As the minimised values of ϵ is the same for all values of n_{i}, one cannot determine this parameter unambiguously. However, this is not an issue for the determination of the reaction rates as $\nu_{\mathrm{Be}\to\mathrm{i}}$ is independent of n_{i} and $\nu_{\mathrm{i}\to\mathrm{Be}}$ does not depend on n_{i} above $\approx 10^{20}$ m^{-2}. Thus, we are using $n_{\mathrm{i}} = 10^{20}$ m^{-2} in the next.

Figure 12 shows the good agreement (below 5% of error) between the RE modelling and the MD simulations with the optimised reaction rates for the Be/BeO(0 0 0 1) interface (a) and the Be/BeO(0 0 0 $\bar{1}$) interface (b) The optimised reaction rates used in these RE modelling are reported in figure 13. They show clear temperature dependencies which are fitted with an Arrhenius law $\nu_{x\to y} = \nu_0 \exp\left(-\frac{E_{x\to y}}{k_{\mathrm{B}}T}\right)$ with the values of ν_0 and $E_{x\to y}$ reported in table 1. For both interfaces, the trapping rates to the interfaces are very similar: the trapping is not affected by the type of interface but rather by the diffusion of D in Be. On the opposite, the detrapping rate from Be/BeO(0 0 0 $\bar{1}$) is lower than the one from Be/BeO(0 0 0 1) which is understandable as the latter trapped more efficiently D at the same temperatures (figure 7). For the Be/BeO(0 0 0 1) interface, the detrapping energy is lower than the trapping energy which may be questionable. This difference is explained by the one order of magnitude lower detrapping pre-exponential factor which keeps the detrapping rate below the trapping rate.

This rate equation modelling suggest that the model presented in the appendix of [47] is able to physically represent the trapping mechanisms happening at he Be/BeO interfaces. The energy barriers reported in table 1, especially the detrapping energies from the interface, may appear small as the typical detrapping energies of D from traps in Be are usually in the 1 eV range [19, 53]. This is due to the low value of the pre-exponential factor ($\approx 10^{10}$ s^{-1}) which are much lower than the one used in rate equation modelling that ranges around 10^{12} or 10^{13} s^{-1} [54, 19, 55]. Such low pre-exponential factors most likely come from the limited range of temperature used in this study. A better assessment of the energy barriers and pre-exponential factors would require MD simulations at much lower temperatures which is technically difficult as the kinetics would most likely be frozen at the MD time scale.

5. Conclusions

Molecular dynamics simulations of D atoms at the Be/BeO interface are presented. The relaxation of the simulation cell without HI shows the presence of

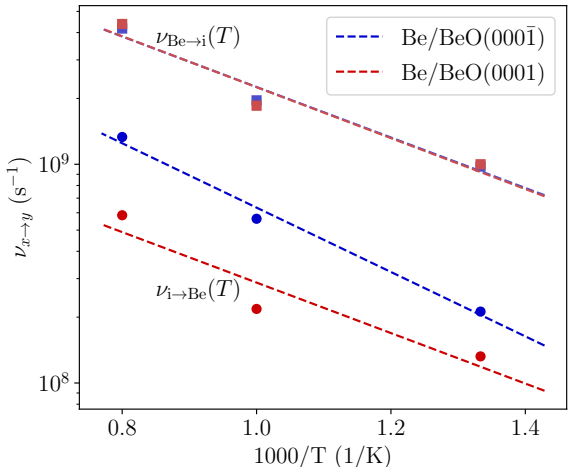

Figure 13: Optimised reaction rates $\nu_{\mathrm{Be}\to\mathrm{i}}$ and $\nu_{\mathrm{i}\to\mathrm{Be}}$ (s^{-1}) used in the rate equation modelling for both interfaces. The dashed line are Arrhenius law $\nu_{x\to y}(T) = \nu_0 \exp\left(-\frac{E_{x\to y}}{k_B T}\right)$ obtained from the rate equation modelling rates.

defects at the Be(0 0 0 1)/BeO(0 0 0 1) interface and the presence of a hexagonal misfit dislocation network at the Be(0 0 0 1)/BeO(0 0 0 $\bar{1}$) interface which creates a pattern of compressed/expanded regions in Be.

Once D atoms are randomly inserted in the Be parts, they tend to be trapped at these defects and in the expanded region of Be leading to an accumulation of D at the interface. No D atom crosses the interface to migrate from the Be part to BeO.

When D atoms are randomly inserted in the BeO part, they initially form O-D bonds. During the simulations, they tend either to be transported to the Be part by crossing the interface or form D_2 molecules (the most stable form of D in BeO). The simulations suggest that once all the atomic D near the interface is consumed by these processes (at 1500 K it happens in about 100 ns), the transport of D across the interface is slowed down: the dissociation of D_2 at the interface blocks the transport of D toward Be. The Be/BeO(0 0 0 1) interface seems also to speed up the formation of D_2 compared to the bulk BeO which suggests the presence of a trap for D_2 at the interface.

In the MD simulations, the kinetics of D concentration in Be and BeO agrees overall with the thermodynamics predictions: when D is in Be, it stays in it and when it is in BeO, it tends to go in Be because the solubility of D in Be is higher than in BeO. This is predicted by the current macroscopic model for D transport in multi-material plasma facing components based on the conservation of the chemical potential. However, our simulations highlight the presence of several kinetic barriers such as traps and D_2 recombination/dissociation at the interface that slow down the path toward the thermodynamic equilibrium. Taking into account these trapping aspects and kinetic barriers may be of importance for assessing the fuel inventory in plasma facing components and to accurately predict the permeation of HI through multi-materials components.

Acknowledgements

This work has been carried out within the framework of the EUROfusion Consortium, funded by the European Union via the Euratom Research and Training Programme (Grant Agreement No 101052200 - EUROfusion). Views and opinions expressed are however those of the author(s) only and do not necessarily reflect those of the European Union or the European Commission. Neither the European Union nor the European Commission can be held responsible for them.
Grants of computer capacity from CSC-IT Center for Science annd the Finnish Grid and Cloud Infrastructure (persistent identifier urn:nbn;fi;research-infras-2016072533) are gratefully acknowledged.
Centre de Calcul Intensif d'Aix-Marseille is acknowledged for granting access to high performance computing ressources.

Appendices

A. Identification of D_2 molecules

Three main types of configurations may exist for D atoms in BeO depending on their environment: D_2 molecules, O-D or Be-D [17]. In Be, Only Be-D exists. For a structure without defect at 0 K, the distinction between these three types of D atoms is straightforward and based on the interatomic distance and the potential energy since each configuration has a given solution energy and geometry. However, the temperature introduces motion and make the determination of configurations harder, especially for D_2 molecules. Here, we describe the method to detect D_2 molecules despite the thermal motion.

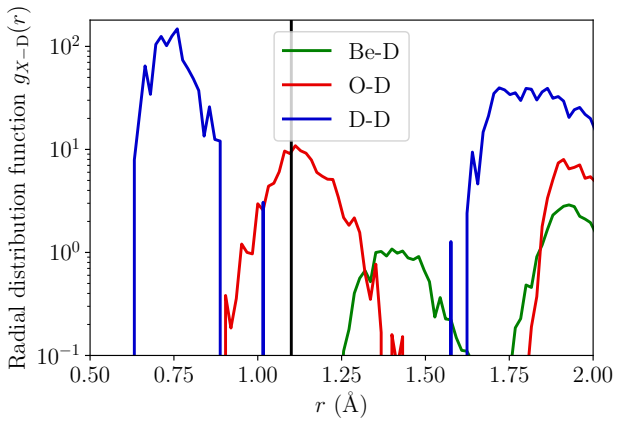

Figure 14: Radial distribution $g_{X-D}(r)$ for D atoms in the last frame of the simulation of D inserted in BeO at 1500 K, calculated by OVITO. The vertical black line at 1.1 Å shows the chosen threshold below which a D_2 molecule is detected in this study.

Figure 14 shows the radial distribution $g_{X-D}(r)$ calculated by OVITO for D atoms in the last frame of the simulation of D inserted in BeO at 1500 K. To detect a D_2 molecule, one can base the analysis on the D-D distance. According to figure 14, there is a first peak around 0.75 Å, corresponding to the D_2 molecules. Then between 1.05 Å and 1.6 Å, $g_{D-D}(r) = 0$. Indeed, according DFT calculations [12] and MD relaxation [17], the stable position for D_2 is in an octahedral position (as defined in [12]). The D_2 molecule is oriented along the **c**-axis in this site. The closest distance between 2 D atoms from 2 molecules in two octahedral neighbour sites is in the **c** direction and is $\frac{c}{2} - \frac{2d_{D-D}}{2} \approx 1.5$ Å with $d_{D-D} \approx 0.75$ Å the bond length of the D_2 molecule in BeO and $c = 4.503$ Å for BeO with the interatomic potential used. Thus, to identify two D atoms in the same octahedral interstitial site that would form a D_2 molecule, the D-D distance needs to be below a cut-off r_{cut,D_2} that is between 1.05 Å and 1.5 Å. With this method, if the D-D distance is below r_{cut,D_2}, both atoms will be counted in the D_2 group independently of their nearest neighbour which could be O or Be due to the thermal motion. The number of calculated D_2 molecules as a function of this cut-off is reported in figure 15. As expected, between 1.00 Å and 1.60 Å, the amount of D_2 stays constant and increases as soon as $r_{cut,D_2} > 1.6$ Å. Thus, a correct value of r_{cut,D_2} to detect D_2 accurately would be between 1.00 Å and 1.60 Å and $r_{cut,D_2} = 1.10$ Å has been chosen.

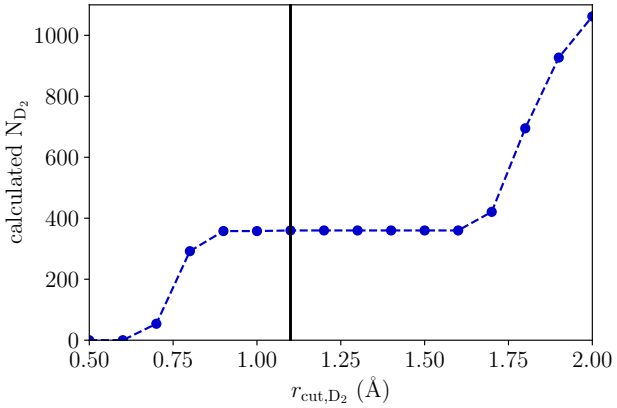

Figure 15: Number of calculated D_2 molecules with our D_2 detection method as a function r_{cut,D_2} for the last frame of the simulation of D inserted in BeO at 1500 K. The vertical line at 1.1 Å shows the chosen threshold below which a D_2 molecule is detected in this study.

As mentioned above, the potential energy could also be used to distinguish between the three categories of D atoms. Figure 16 shows the distribution of D atoms as a function of E_{pot} for the last frame of the simulation of D inserted in BeO at 1500 K. The D atoms are also sorted in the three categories D_2, O-D and Be-D in order to see if it is possible to distinguish the D atoms based on their potential energy. The distribution of D_2 peaks for the lowest E_{pot} around -2.37 eV/atoms showing that D seems to be the most stable configuration in BeO. However, the distributions of O-D and Be-D, peaking above 2.0 eV/atom are broad and overlap with the one of D_2 (thermal motion and defects at the interface). In addition, the distribution of D_2 extends quite high in the potential energy, up to -2.0 eV/atom (this tail also occurs for $r_{cut,D_2} = 0.8$ Å). Thus, the distinction between the three configuration based on the potential energy is not possible.

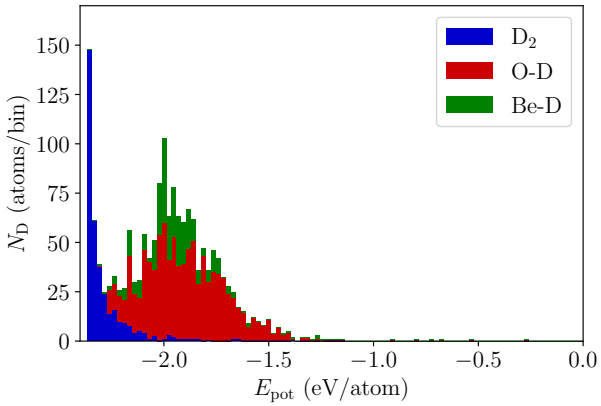

Figure 16: Distribution of D atoms as a function of E_{pot} (100 bins between -2.37 eV and 0 eV) for the last frame of the simulation of D inserted in BeO at 1500 K. The D atoms are also sorted in the three categories D_2, O-D and Be-D. 0 eV potential energy represents an atom which is not bound to any other atoms (in the cutoff range of the interatomic potentials).

References

[1] V. Philipps, Ph. Mertens, G.F. Matthews, and H. Maier. Overview of the jet iter-like wall project. *Fusion Engineering and Design*, 85(7):1581 – 1586, 2010. Proceedings of the Ninth International Symposium on Fusion Nuclear Technology.

[2] S. Brezinsek. Plasma-surface interaction in the be/w environment: Conclusions drawn from the jet-ilw for iter. *Journal of Nuclear Materials*, 463:11 – 21, 2015. PLASMA-SURFACE INTERACTIONS 21.

[3] A. Loarte, B. Lipschultz, A.S. Kukushkin, G.F. Matthews, P.C. Stangeby, N. Asakura, G.F. Counsell, G. Federici, A. Kallenbach, K. Krieger, A. Mahdavi, V. Philipps, D. Reiter, J. Roth, J. Strachan, D. Whyte, R. Doerner, T. Eich, W. Fundamenski, A. Herrmann, M. Fenstermacher, P. Ghendrih, M. Groth, A. Kirschner, S. Konoshima, B. LaBombard, P. Lang, A.W. Leonard, P. Monier-Garbet, R. Neu, H. Pacher, B. Pegourie, R.A. Pitts, S. Takamura, J. Terry, E. Tsitrone, the ITPA Scrape-off Layer, and Divertor Physics Topical Group. Chapter 4: Power and particle control. *Nuclear Fusion*, 47(6):S203, 2007.

[4] K. Heinola, A. Widdowson, J. Likonen, E. Alves, A. Baron-Wiechec, N. Barradas, S. Brezinsek, N. Catarino, P. Coad, S. Koivuranta, G.F. Matthews, M. Mayer, and P. Petersson. Fuel retention in jet iter-like wall from post-mortem analysis. *Journal of Nuclear Materials*, 463:961 – 965, 2015. PLASMA-SURFACE INTERACTIONS 21.

[5] S. Brezinsek, T. Loarer, V. Philipps, H.G. Esser, S. Grünhagen, R. Smith, R. Felton, J. Banks, P. Belo, A. Boboc, J. Bucalossi, M. Clever, J.W. Coenen, I. Coffey, S. Devaux, D. Douai, M. Freisinger, D. Frigione, M. Groth, A. Huber, J. Hobirk, S. Jachmich, S. Knipe, K. Krieger, U. Kruezi, S. Marsen, G.F. Matthews, A.G. Meigs, F. Nave, I. Nunes, R. Neu, J. Roth, M.F. Stamp, S. Vartanian, U. Samm, and JET EFDA contributors. Fuel retention studies with the iter-like wall in jet. *Nuclear Fusion*, 53(8):083023, 2013.

[6] C. Grisolia. Plasma wall interaction during long pulse operation in tore supra. *Journal of Nuclear Materials*, 266-269:146 – 152, 1999.

[7] M. G. Ganchenkova, V. A. Borodin, and R. M. Nieminen. Hydrogen in beryllium: Solubility, transport, and trapping. *Phys. Rev. B*, 79:134101, Apr 2009.

[8] S.C. Middleburgh and R.W. Grimes. Defects and transport processes in beryllium. *Acta Materialia*, 59(18):7095 – 7103, 2011.

[9] Pengbo Zhang, Jijun Zhao, and Bin Wen. Retention and diffusion of h, he, o, c impurities in be. *Journal of Nuclear Materials*, 423(1):164 – 169, 2012.

[10] L. Ferry, F. Virot, Y. Ferro, D. Matveev, Ch. Linsmeier, and M. Barrachin. Diffusivity of hydrogen and properties of point defects in beryllium investigated by dft. *Journal of Nuclear Materials*, 524:323 – 329, 2019.

[11] A. G. Marinopoulos, R. C. Vilão, R. B. L. Vieira, H. V. Alberto, J. M. Gil, M. V. Yakushev, R. Scheuermann, and T. Goko. Defect levels and hyperfine constants of hydrogen in beryllium oxide from hybrid-functional calculations and muonium spectroscopy. *Philosophical Magazine*, 97(24):2108–2128, 2017.

[12] Etienne A Hodille, Yves Ferro, Zachary Piazza, and Cédric Pardanaud. Hydrogen in beryllium oxide investigated by DFT: on the relative stability of charged-state atomic versus molecular hydrogen. *Journal of Physics: Condensed Matter*, 2018.

[13] Ch. Stihl, P.V. Vladimirov, and A. Möslang. Assessment of multiscale hydrogen desorption models from (0001) be surfaces. *Journal of Nuclear Materials*, 543:152595, 2021.

[14] C Björkas, D Borodin, A Kirschner, R K Janev, D Nishijima, R Doerner, and K Nordlund. Molecules can be sputtered also from pure metals: sputtering of beryllium hydride by fusion plasma–wall interactions. *Plasma Physics and Controlled Fusion*, 55(7):074004, 2013.

[15] E. Safi, C. Björkas, A. Lasa, K. Nordlund, I. Sukuba, and M. Probst. Atomistic simulations of the effect of reactor-relevant parameters on be sputtering. *Journal of Nuclear Materials*, 463:805–809, 2015. PLASMA-SURFACE INTERACTIONS 21.

[16] E Safi, G Valles, A Lasa, and K Nordlund. Multi-scale modelling to relate beryllium surface temperature, deuterium concentration and erosion in fusion reactor environment. *Journal of Physics D: Applied Physics*, 50(20):204003, 2017.

[17] E A Hodille, J Byggmästar, E Safi, and K Nordlund. Molecular dynamics simulation of beryllium oxide irradiated by deuterium ions: sputtering and reflection. *Journal of Physics: Condensed Matter*, 31(18):185001, mar 2019.

[18] E A Hodille, J Byggmästar, E Safi, and K Nordlund. Sputtering of beryllium oxide by deuterium at various temperatures simulated with molecular dynamics. *Physica Scripta*, T171:014024, jan 2020.

[19] D. Matveev, M. Wensing, L. Ferry, F. Virot, M. Barrachin, Y. Ferro, and Ch. Linsmeier. Reaction-diffusion modeling of hydrogen transport and surface effects in application to single-crystalline be. *Nuclear Instruments and Methods in Physics Research Section B: Beam Interactions with Materials and Atoms*, 430:23 – 30, 2018.

[20] M. Kumar, C. Makepeace, C. Pardanaud, Y. Ferro, E. Hodille, C. Martin, P. Roubin, A. Widdowson, T. Dittmar, C.h. Linsmeier, C.P. Lungu, C. Porosnicu, I. Jepu, P. Dinca, M. Lungu, O.G. Pompilian, and JET contributors. Identification of beo and beoxdy in melted zones of the jet be limiter tiles: Raman study using comparison with laboratory samples. *Nuclear Materials and Energy*, 17:295 – 301, 2018.

[21] Makepeace C., Pardanaud C., Roubin P., Borodkina I., Ayres C., Coad P., Baron-Wiechec A., Jepu I., Heinola K., Widdowson A., Lozano-Perez S., and J.E.T. Contributors . The effect of beryllium oxide on retention in JET ITER-like wall tiles. *Nuclear Materials and Energy*, 19:346–351, 2019.

[22] Sung Man Lee and Jai Young Lee. The effect of the interface character of tic particles on hydrogen trapping in steel. *Acta Metallurgica*, 35(11):2695–2700, 1987.

[23] Wei F.G and Tsuzaki K. Quantitative analysis on hydrogen trapping of tic particles in stells. *Metallurgical and Materials Transactions A*, 37:331–353, 2006.

[24] Rongjian Shi, Yuan Ma, Zidong Wang, Lei Gao, Xu-Sheng Yang, Lijie Qiao, and Xiaolu Pang. Atomic-scale investigation of deep hydrogen trapping in nbc/alpha-fe semi-coherent interfaces. *Acta Materialia*, 200:686–698, 2020.

[25] A.A. Mirzoev, A.V. Verkhovykh, and D.A. Mirzaev. Ab initio modelling of the hydrogen interaction with ferrite/cementite interface. *Procedia Engineering*, 214:9–17, 2017.

[26] L. Yang and B. D. Wirth. First-principles study of hydrogen behavior near w/wc interfaces. *Journal of Applied Physics*, 127(11):115107, Mar 2020.

[27] Jingming Shi, Naoyuki Hashimoto, and Shigehito Isobe. Behavior of hydrogen at fe/w interface: a first-principle calculation study. *Journal of Nuclear Science and Technology*, 57(11):1223–1230, Nov 2020.

[28] Xiao Liu, Huaican Chen, Jianfei Tong, Wenhao He, Xujing Li, Tianjiao Liang, Yuhong Li, and Wen Yin. The kinetic behaviors of h impurities in the li/ta bilayer: Application for the accelerator-based bnct. *Nanomaterials*, 9(8):1107, Aug 2019.

[29] Gui-Yang Huang, Xunxiang Hu, and Brian D Wirth. First-principles investigations of hydrogen trapping in y 2 o 3 and the y 2 o 3 —bcc fe interface. *Journal of Physics: Condensed Matter*, 32(49):495001, Nov 2020.

[30] V. D. Scott. Structure and growth of beryllium oxide on single crystal of beryllium. *Acta Crystallographica*, 12(2):136–142, Feb 1959.

[31] C. Björkas, N. Juslin, H. Timko, K. Vörtler, K. Nordlund, K. Henriksson, and P. Erhart. Interatomic potentials for the Be-C-H system. *Journal of Physics: Condensed Matter*, 21(44):445002, 2009.

[32] J Byggmästar, E A Hodille, Y Ferro, and K Nordlund. Analytical bond order potential for simulations of BeO 1D and 2D nanostructures and plasma-surface interactions. *Journal of Physics: Condensed Matter*, 30(13):135001, 2018.

[33] K. Nordlund, M. Ghaly, R. S. Averback, M. Caturla, T. Diaz de la Rubia, and J. Tarus. Defect production in collision cascades in elemental semiconductors and fcc metals. *Phys. Rev. B*, 57:7556–7570, Apr 1998.

[34] Alexander Stukowski. Visualization and analysis of atomistic simulation data with ovito–the open visualization tool. *Modelling and Simulation in Materials Science and Engineering*, 18(1):015012, 2010.

[35] J. D. Hunter. Matplotlib: A 2d graphics environment. *Computing in Science & Engineering*, 9(3):90–95, 2007.

[36] J. Tersoff. New empirical model for the structural properties of silicon. *Phys. Rev. Lett.*, 56:632–635, Feb 1986.

[37] J. Tersoff. New empirical approach for the structure and energy of covalent systems. *Phys. Rev. B*, 37:6991–7000, Apr 1988.

[38] Donald W. Brenner. Empirical potential for hydrocarbons for use in simulating the chemical vapor deposition of diamond films. *Phys. Rev. B*, 42:9458–9471, Nov 1990.

[39] Paul Erhart, Niklas Juslin, Oliver Goy, Kai Nordlund, Ralf Müller, and Karsten Albe. Analytic bond-order potential for atomistic simulations of zinc oxide. *Journal of Physics: Condensed Matter*, 18(29):6585, July 2006.

[40] J Byggmästar, M Nagel, K Albe, K O E Henriksson, and K Nordlund. Analytical interatomic bond-order potential for simulations of oxygen defects in iron. *Journal of Physics: Condensed Matter*, 31(21):215401, mar 2019.

[41] H. J. C. Berendsen, J. P. M. Postma, W. F. van Gunsteren, A. DiNola, and J. R. Haak. Molecular dynamics with coupling to an external bath. *The Journal of Chemical Physics*, 81(8):3684–3690, 1984.

[42] Alexander Stukowski, Vasily V Bulatov, and Athanasios Arsenlis. Automated identification and indexing of dislocations in crystal interfaces. *Modelling and Simulation in Materials Science and Engineering*, 20(8):085007, oct 2012.

[43] Wei Yang, Georges Ayoub, Iman Salehinia, Bilal Mansoor, and Hussein Zbib. Multiaxial tension/compression asymmetry of ti/tin nano laminates: Md investigation. *Acta Materialia*, 135:348 – 360, 2017.

[44] Wei Yang, Georges Ayoub, Iman Salehinia, Bilal Mansoor, and Hussein Zbib. Deformation mechanisms in ti/tin multilayer under compressive loading. *Acta Materialia*, 122:99 – 108, 2017.

[45] Changsoo Jang, Seungbae Park, Bongtae Han, and Samson Yoon. Advanced Thermal-Moisture Analogy Scheme for Anisothermal Moisture Diffusion Problem. *Journal of Electronic Packaging*, 130(1), 01 2008. 011004.

[46] Dapeng Liu, Jing Wang, Ruiyang Liu, and S.B. Park. An examination on the direct concentration approach to simulating moisture diffusion in a multi-material system. *Microelectronics Reliability*, 60:109 – 115, 2016.

[47] Rémi Delaporte-Mathurin, Etienne A. Hodille, Jonathan Mougenot, Yann Charles, Gregory De Temmerman, Floriane Leblond, and Christian Grisolia. Influence of interface conditions on hydrogen transport studies. *Nuclear Fusion*, 61(3):036038, feb 2021.

[48] R. Arredondo, K. Schmid, F. Subba, and G.A. Spagnuolo. Preliminary estimates of tritium permeation and retention in the first wall of demo due to ion bombardment. *Nuclear Materials and Energy*, 28:101039, 2021.

[49] A. Allouche and Y. Ferro. First-Principles Study of hydrogen retention and diffusion in beryllium oxide. *Solid State Ionics*, 272:91–100, 2015.

[50] Rémi Delaporte-Mathurin, Etienne A. Hodille, Jonathan Mougenot, Yann Charles, and Christian Grisolia. Parametric optimisation based on tds experiments for rapid and efficient identification of hydrogen transport materials properties. *Nuclear Materials and Energy*, 27:100984, 2021.

[51] Pauli Virtanen, Ralf Gommers, Travis E. Oliphant, Matt Haberland, Tyler Reddy, David Cournapeau, Evgeni Burovski, Pearu Peterson, Warren Weckesser, Jonathan Bright, Stéfan J. van der Walt, Matthew Brett, Joshua Wilson, K. Jarrod Millman, Nikolay Mayorov, Andrew R. J. Nelson, Eric Jones, Robert Kern, Eric Larson, C. J. Carey, İlhan Polat, Yu Feng, Eric W. Moore, Jake VanderPlas, Denis Laxalde, Josef Perktold, Robert Cimrman, Ian Henriksen, E. A. Quintero, Charles R. Harris, Anne M. Archibald, Antônio H. Ribeiro, Fabian Pedregosa, and Paul van Mulbregt. SciPy 1.0: fundamental algorithms for scientific computing in Python. *Nature Methods*, 17(3), March 2020.

[52] Eric Jones, Travis Oliphant, Pearu Peterson, et al. SciPy: Open source scientific tools for Python, 2001–. [Online; accessed 2018-08-10].

[53] M.J. Baldwin, T. Schwarz-Selinger, and R.P. Doerner. Experimental study and modelling of deuterium thermal release from be–d co-deposited layers. *Nuclear Fusion*, 54(7):073005, apr 2014.

[54] E.A. Hodille, A. Založnik, S. Markelj, T. Schwarz-Selinger, C.S. Becquart, R. Bisson, and C. Grisolia. Simulations of atomic deuterium exposure in self-damaged tungsten. *Nuclear Fusion*, 57(5):056002, mar 2017.

[55] K Schmid, J Bauer, T Schwarz-Selinger, S Markelj, U v Toussaint, A Manhard, and W Jacob. Recent progress in the understanding of h transport and trapping in w. *Physica Scripta*, T170:014037, oct 2017.